

Heat transfer in flow around a rotary oscillating cylinder at a high subcritical Reynolds number

A computational study

Hadžiabdić, M.; Palkin, E.; Mullyadzhanov, R.; Hanjalić, K.

DOI

[10.1016/j.ijheatfluidflow.2019.108441](https://doi.org/10.1016/j.ijheatfluidflow.2019.108441)

Publication date

2019

Document Version

Final published version

Published in

International Journal of Heat and Fluid Flow

Citation (APA)

Hadžiabdić, M., Palkin, E., Mullyadzhanov, R., & Hanjalić, K. (2019). Heat transfer in flow around a rotary oscillating cylinder at a high subcritical Reynolds number: A computational study. *International Journal of Heat and Fluid Flow*, 79, Article 108441. <https://doi.org/10.1016/j.ijheatfluidflow.2019.108441>

Important note

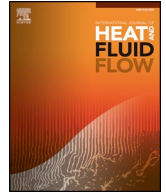
To cite this publication, please use the final published version (if applicable). Please check the document version above.

Copyright

Other than for strictly personal use, it is not permitted to download, forward or distribute the text or part of it, without the consent of the author(s) and/or copyright holder(s), unless the work is under an open content license such as Creative Commons.

Takedown policy

Please contact us and provide details if you believe this document breaches copyrights. We will remove access to the work immediately and investigate your claim.



Heat transfer in flow around a rotary oscillating cylinder at a high subcritical Reynolds number: A computational study



M. Hadžiabdić^{*,a}, E. Palkin^{b,c}, R. Mullyadzhyanov^{b,c}, K. Hanjalić^{d,e}

^a International University of Sarajevo, Hrasnička cesta 15, Ilidža, Sarajevo 71210, Bosnia and Herzegovina

^b Institute of Thermophysics SB RAS, Lavrentyev str. 1, Novosibirsk 630090, Russia

^c Novosibirsk State University, Pirogov str. 2, Novosibirsk 630090, Russia

^d Delft University of Technology, Bld. 58, Van der Maasweg 9, Delft 2629 HZ, the Netherlands

^e University of Sarajevo, Vilsonovo šetalište 8, Sarajevo 71000, Bosnia and Herzegovina

ARTICLE INFO

Keywords:

Rotating cylinder
URANS
Flow control
Heat transfer

ABSTRACT

We studied numerically the heat transfer in flow over a rotationally oscillating cylinder at a subcritical Reynolds number ($Re = 1.4 \times 10^5$) that is an order of magnitude higher than previously reported in the literature. This paper is a follow-up of the earlier study of hydrodynamics and drag force in a range of forcing frequencies and amplitudes (Palkin et al., 2018). This time we focus on heat transfer and its correlation with the observed flow field and vortical patterns. Four forcing frequencies $f = f_c/f_0 = 0, 1, 2.5, 4$ for two forcing amplitudes $\Omega = \Omega_c D/2U_\infty = 1$ and 2 are considered, where f_0 is the natural vortex-shedding frequency, U_∞ the free-stream velocity and D the cylinder diameter. The parametric study was performed by solving three-dimensional unsteady Reynolds-averaged Navier–Stokes (URANS) equations closed by a wall-integrated second-moment (Re-stress) model, verified earlier by Large-eddy simulations and experiments in several reference cases including flows over a stagnant, as well as rotary oscillating cylinders at the same Re number. The thermal field, treated as a passive scalar, was obtained from the simultaneous solution of the energy equation, closed by the standard (GGDH) anisotropic eddy-diffusivity model. The computations showed that for the unforced cylinder heat transfer is characterized by very high local rates due to a strong thinning of the thermal boundary layer as a result of the impact and interactions of large coherent structures with the wall. The overall average Nusselt number does not change much for the forced cylinder but its time-averaged, phase-averaged and instantaneous circumferential profiles show some profound differences compared to the stationary cylinder. The distribution of Nu on the back surface becomes more uniform with less frequent occurrence of high values, especially for the higher frequencies $f = 2.5$ and $f = 4$. This is attributed to diminishing of the mean-recirculation zone as well as to the overall suppression of turbulent fluctuations. The rotary oscillation of the cylinder appears potentially efficient in achieving a more uniform circumferential distribution of Nu and avoiding local overheats and hot spots.

1. Introduction

Fluid flows over bluff bodies continue to attract attention among research and engineering communities. The drag and lift forces acting on the body due to periodic formation and shedding of large-scale vortices lead to flow-induced vibrations and can cause serious structural damages. Heat transfer between bodies and fluid in such flow configurations is also of interest in a number of engineering applications such as design of efficient heat exchangers. Effective and cost-benefit control and manipulations of flow-induced drag, lift and heat transfer require prior thorough understanding of flow, turbulence and

vortex dynamics, which are usually studied in simple generic situations easily manageable by experiments and computer simulations, as found in a wealth of the literature on this topic. A canonical case of flow over a circular cylinder often serves as a paradigm of bluff body configuration. The hydrodynamics of the case is well studied both experimentally and numerically. First experiments were performed by Wieselsberger (1922), Fage (1929), Roshko (1954), Bloor (1964), Williamson (1988), among others. Roshko measured the case up to the Reynolds number 10^4 reporting on the turbulent Kármán vortex street for $Re > 300$. Roshko (1961) also extended the lower Reynolds numbers investigations showing an abrupt decrease of the drag coefficient

* Corresponding author.

E-mail addresses: mhadziabdic@ius.edu.ba (M. Hadžiabdić), rustammul@gmail.com (R. Mullyadzhyanov).

<https://doi.org/10.1016/j.ijheatfluidflow.2019.108441>

Received 31 January 2019; Received in revised form 6 July 2019; Accepted 10 July 2019

Available online 17 July 2019

0142-727X/ © 2019 Elsevier Inc. All rights reserved.

at $2 \times 10^5 < Re < 5 \times 10^5$ and its subsequent increase at $10^6 < Re < 3.5 \times 10^6$.

Numerical studies started with a two-dimensional (2D) steady-state direct numerical simulation (DNS) at low Reynolds numbers $Re = 10, 20$ by Thom (1933). More recent unsteady simulations pushed the Reynolds number up to $Re = 10^2 - 10^7$ (Singh and Mittal, 2005). These studies provided a better understanding of the flow features and different regimes. However, the turbulent flow is essentially three-dimensional motivating full scale investigations. First 3D direct numerical simulation where transverse direction was taken into account has been performed by Karniadakis and Triantafyllou (1992) in the range of $Re = 200 - 500$. Recently, Lehmkühl et al. (2014), Rodríguez et al. (2015) and Cheng et al. (2017) studied the flow in the range of Reynolds numbers up to 8.5×10^5 with the well-resolved Large-eddy simulations (LES) and clarified several issues of the drag crisis phenomenon. The first calculations of the heat transfer also started with the steady case at low Reynolds numbers ($Re \leq 40$). Recently, Bouhairie and Chu (2007) increased Re up to 1.56×10^4 in the 2D framework. The first 3D simulations were performed by Xia and Karniadakis (1997) at $Re = 500$ and 3900 using LES.

Experimental measurements of the flow over a heated cylinder were pioneered by Hilpert (1933), Small (1935) and Kruzhilin (1936), among others. Extensive reviews are provided by Žukauskas (1972), Morgan (1975) and Sparrow et al. (2004). An important issue concerning the heat transfer is the influence of thermal boundary conditions on the cylinder wall which usually boils down to the constant wall temperature (CWT) or constant heat flux (CHF) condition. Boulos and Pei (1974) found that the overall heat transfer differed within 10 – 20% between CWT and CHF conditions for $Re < 10^4$. Similar results were obtained by Papell (1981) and Baughn and Saniei (1991). At relatively low Reynolds numbers the heat transfer coefficient reaches its maximum at the frontal stagnation point. However, at $Re > 5.0 \times 10^4$, it becomes higher in the rear portion of the cylinder due to the intensive turbulent fluctuations in the near wake (Schmidt and Wenner, 1941). Thus, the point of laminar-turbulent transition is crucial for the correct heat transfer description. This feature is also reflected in empirical correlations which are usually composed of two terms (Perkins Jr and Leppert, 1964), i.e. the laminar contribution from the front part of the cylinder where the Nusselt number depends as $Re^{1/2}$ and the turbulent part where $Nu \propto Re^{2/3}$. Thus, a promising way to affect the heat transfer is to manipulate the boundary layer of the flow.

There are many ways to affect the flow and heat transfer around cylinder, such as the application of blowing/suction of the fluid through the cylinder wall, distributed forcing, various geometric modifications including roughness, dimples, splitter plates, grooves, small secondary cylinder, electromagnetic forcing, hydrophobic surfaces, steady and oscillating rotation, in-line and transverse oscillations, etc (Choi et al., 2008). Aside from manipulating forces acting on the bluff body, large part of research targets the heat transfer processes. Here we mainly review the work based on the oscillations of the cylinder of different kinds. Harmonic oscillations impose a certain frequency leading to the synchronization of the vortex shedding process with external forcing. This phenomenon is known as the lock-on which provides the increase of drag and lift as the typical vortical structures shed from the cylinder are significantly intensified. This inevitably affects the heat transfer. Extensive research has been devoted to transverse and in-line oscillations, e.g. Lemlich (1955), Zijnen (1958), Lemlich and Levy (1961), Sreenivasan and Ramachandran (1961), Deaver et al. (1962), Jameson (1964), Lemlich and Rao (1965), Faircloth and Schaetzle (1969), Armaly and Madsen (1971), Saxena and Laird (1978), Leung et al. (1981), Karanth et al. (1994), Cheng et al. (1997), Gau et al. (1999), Park and Gharib (2001), Fu and Tong (2002), Pottebaum and Gharib (2006), Nobari and Ghazanfarian (2010), Al-Mdallal and Mahfouz (2017), among others. A typical conclusion here is the notable intensification of heat transfer near the lock-on boundary.

Another appealing method to control the flow is the rotary oscillations of the cylinder. This method is known by the pioneering experiments of Tokumaru and Dimotakis (1991) whose results were later confirmed by two-dimensional numerical simulations of Shiels and Leonard (2001). They showed that the drag and lift coefficients and their fluctuations can be significantly damped at $Re \sim 10^4$ depending on the frequency and amplitude of the oscillations. Three-dimensional simulations were performed by Aguedal et al. (2018) and Du and Dalton (2013) for $Re = 3900$ and 1.5×10^4 , respectively, drawing similar conclusions. The corresponding heat transfer problem has been studied by Mahfouz and Badr (1999), Mahfouz and Badr (2000), Sellappan and Pottebaum (2014) and Mittal and Al-Mdallal (2018) mainly targeting low Reynolds number range. They found that the vortex shedding influences the thermal field in the wake region and also observed a significant heat-transfer enhancement in the lock-on region. One application of the present method is the heat/mixing transfer intensification in a plane channel with the oscillating cylinder placed in the middle. This configuration has been studied in a series of papers by Celik et al. (2008), Celik and Beskok (2009), Beskok et al. (2012). Recently, we have extended results of Tokumaru and Dimotakis (1991) to an order of magnitude higher $Re = 1.4 \times 10^5$ showing that the method becomes even more effective to suppress drag and lift oscillations (Palkin et al., 2018).

We study the effect of cylinder rotary oscillations on the heat transfer by performing unsteady RANS computations at a high sub-critical Reynolds number $Re = 1.4 \times 10^5$ which is at least an order of magnitude higher than previously explored in the literature. The tangential velocity of the cylinder wall is forced to oscillate in time according to

$$\frac{U_w}{U_\infty} = \Omega^* \sin(2\pi f_e^* t^*) = \Omega^* \sin(\varphi^*), \quad (1)$$

where f_e is the imposed frequency, the angular velocity ω_e represents the amplitude of oscillations, $\Omega^* = \omega_e D / 2U_\infty = \Omega_e / U_\infty$, $t^* = tU_\infty / D$ is the non-dimensional amplitude, $f_e^* = f_e D / U_\infty$ is the Strouhal number of the imposed oscillations, $\varphi^* = 2\pi f_e^* t^*$ is the rotational phase, D is the cylinder diameter and U_∞ is the uniform inflow velocity. For clarity, in the further text we deleted the subscripts and consider all variables as nondimensional. We studied the range of parameters $\Omega = 1, 2$ and $f = f_e / f_0 = 1, 2.5$ and 4 , where f_0 is the natural vortex-shedding frequency at this Reynolds number. However, motivated by the earlier findings that high frequencies bring more efficient suppression of drag and lift forces, we consider here only high-frequency forcing that go beyond the lock-on conditions (f less than 1). The research focus is the modification of the Nusselt number due to oscillatory rotation defined as

$$Nu = \frac{hD}{\lambda}, \quad (2)$$

where λ is the thermal conductivity of the fluid and h is the heat transfer coefficient.

2. Computational details and model validation

Fig. 1 shows the computational domain and imposed boundary conditions. The spanwise length was $L_z = 2D$ while the streamwise and crosswise dimensions were $L_x \times L_y = 25D \times 20D$. The uniform velocity U_∞ , zero free-stream turbulence and constant temperature T_∞ were imposed at the inflow while the no-slip boundary condition was imposed at the cylinder wall with the time-dependent tangential velocity calculated every time step according to Eq. (1) and constant heat flux (CHF) for the temperature field. The lateral sides were considered as periodic faces while a slip condition was set at the top and bottom boundaries with convective outflow at the outlet boundary. All computations were carried out on a mesh containing 2.24×10^6 cells which

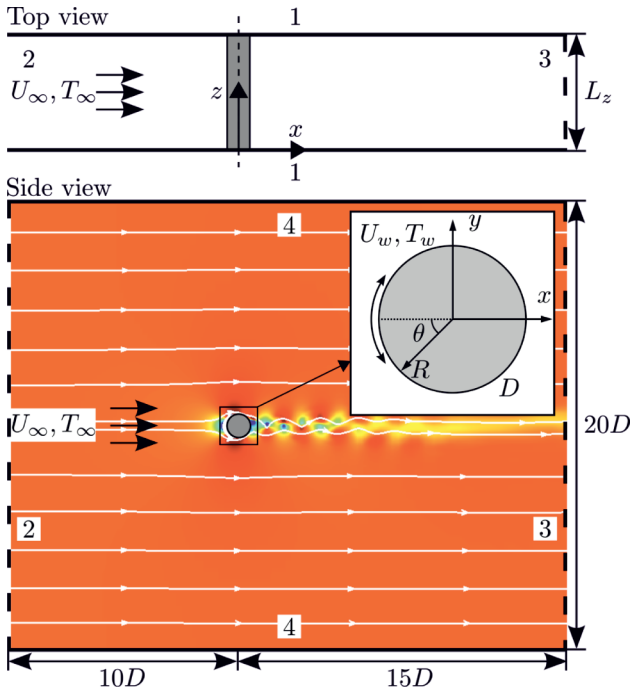


Fig. 1. Computational domain with a schematic picture of the flow over an oscillating cylinder: 1 – periodic, 2 – inflow, 3 – convective outflow and 4 – slip boundary condition.

was carefully designed to ensure a fine resolution in the regions of large gradients as well as in the areas of anticipated flow separation. The radial and circumferential cell dimensions in terms of wall units (friction velocity and viscosity) were $\Delta r^+ < 3$ and $(R\Delta\theta)^+ < 70$ for the area before separation and $\Delta r^+ < 1.0 - 1.8$ and $(R\Delta\theta)^+ < 40$ after the separation computed for the non-rotating case (Palkin et al., 2018). Note that all the values further were non-dimensionalized using D , U_∞ and T_∞ resulting in the following non-dimensional parameters:

$$Re = \frac{U_\infty D}{\nu}, \quad Pr = \frac{\nu}{\lambda} \quad (3)$$

$$Nu = Re Pr \frac{q_w}{U_\infty (T_w - T_\infty)}, \quad (4)$$

where ν is the kinematic viscosity of the fluid, T the temperature, T_w the local temperature at the wall of the cylinder where constant heat flux q_w was imposed. The present results were obtained for $Re = 1.4 \times 10^5$ and $Pr = 0.71$.

The URANS computations were performed using an open source in-house unstructured finite-volume code T-Flows (Ničeno and Hanjalić, 2005; Ničeno et al., 2018) that was successfully applied in different (U) RANS, LES and hybrid LES/RANS computations (Hadžiabdić and Hanjalić, 2008; Manceau et al., 2014; Palkin et al., 2016). The code features second-order accuracy schemes for the diffusion and convection terms in the momentum and energy equations, whereas the time-marching was performed using a fully-implicit three-level time scheme. The wall-integrated Reynolds Stress Model (RSM HJ) of Jakirlić and Hanjalić (2002) was used to close the momentum equation in the URANS framework. The general gradient diffusion hypothesis (GGDH) was used to model the turbulent heat flux to close the energy equation:

$$\widetilde{u_i \theta} = C_\theta \frac{k}{\varepsilon} \widetilde{u_i} \frac{\partial \widetilde{T}}{\partial x_j}, \quad (5)$$

where the tilde denotes the ensemble-averaging used by URANS, u_i and θ are the components of the velocity and temperature fluctuations, k the modelled turbulent kinetic energy, ε the dissipation of turbulent kinetic

energy, and the coefficient C_θ was set to 0.15.¹ Furthermore, in order to improve the prediction of heat transfer we introduced a realizability time-scale limiter in the dissipation-rate equation proposed by Medic and Durbin (2002):

$$\tau = \min\left(\frac{k}{\varepsilon}, \frac{\alpha}{\sqrt{6} C_\mu |\widetilde{S}|}\right), \quad (6)$$

where C_μ is the standard eddy viscosity coefficient ($= 0.09$) and $|\widetilde{S}|$ the magnitude of the rate-of-strain tensor. The coefficient α is equal to 1 in the original derivation of Durbin (1996), but increased here up to 1.2 in order to extend the region where the original definition of time scale (k/ε) is applied. The time limiter is activated in a few spots where very high values of turbulent heat flux occur.

2.1. Validation of velocity field

In our preceding works (Palkin et al., 2016; 2018), URANS with RSM HJ model proved to be capable of reproducing all important flow features around non-rotating and rotary oscillating cylinder in accord with the LES and the available experiments for several reference cases. For the non-rotating cylinder the time-averaged value of the drag coefficient ($\overline{C_D}$) = 1.24 agreed very well with the experimental value $\langle C_D \rangle = 1.23$ reported by Cantwell and Coles (1983). Note that the overline denotes the time-averaging, while $\langle \rangle$ corresponds to the averaging over the surface of the cylinder. Palkin et al. (2018) performed two additional LES simulations of rotary oscillating cylinder for two sets of parameters, $f = 2.5$, $\Omega = 2$ and $f = 4$, $\Omega = 2$ in order to evaluate the performance of RSM HJ in that case. Similarly to non-rotating cases, URANS produced results that were in good agreement with the reference LES results both for the mean velocity field, see Fig. 2 (left), but also for the dynamic features of the flow assessed by comparing the drag and lift coefficients, shown in Fig. 2 (right).

The heat transfer is analyzed for 7 cases, i.e. the flow around a stationary cylinder and six cases of rotary oscillating cylinder with rotational amplitude $\Omega = 1$ and 2 for frequencies $f = 1, 2.5$ and 4. For the combinations of the above values of f and Ω the arc length traveled by a particle fixed on the cylinder surface during half of the oscillation period were calculated from:

$$L = \int_0^{1/2f_c} U_w dt = \frac{\Omega}{\pi f_c} = \frac{1}{\pi f_0} \frac{\Omega}{f}, \quad (7)$$

where $\pi f_0 \approx 0.682$ and U_w is defined by Eq. (1). For Ω/f taking minimum and maximum values ($\Omega = 1$, $f = 4$ and $\Omega = 2$, $f = 1$) the arc length values are 0.367 and 2.934, respectively. The minimum and maximum ratio of the arc length to the perimeter of the cylinder results in 0.117 and 0.934, respectively.

2.2. Validation of thermal field

In order to proceed with the further analysis, we validate our simulations of the temperature field. The case without rotation has been extensively studied in the literature. However, the distribution of the Nusselt number on the surface appears to be very sensitive to a number of factors, such as the inflow turbulence level (Sak et al., 2007) or the aspect ratio of the channel (Chang and Mills, 2004). As mentioned in the Introduction, at the front part of the cylinder where the flow in subcritical regime is laminar the Nusselt number increases as $Re^{1/2}$, while on the rear cylinder surface subjected to turbulence, heat transfer coefficient follows a $Nu \propto Re^{2/3}$ correlation. Fig. 3 shows the variation of

¹The adopted $C_\theta = 0.15$, though found in the literature (Ince and Launder, 1989), is smaller than the common 0.3 value estimated from the near-wall equilibrium conditions and used in steady RANS computations (Thielen et al., 2005). In the URANS approach the total turbulent heat flux is a sum of modeled and resolved part, justifying a lower value of C_θ .

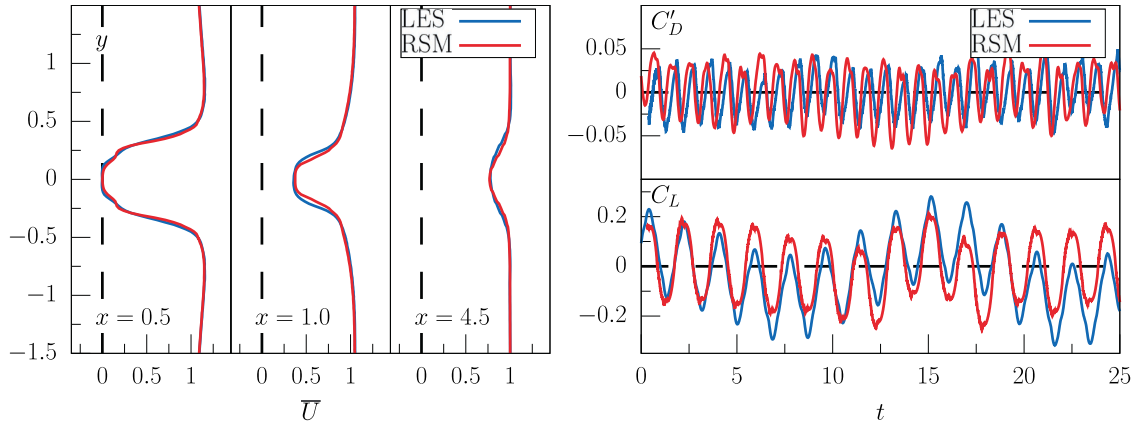


Fig. 2. Left: Time-averaged streamwise velocity profiles at several locations downstream. Right: Time evolution of the drag coefficient fluctuations $C'_D = C_D - \bar{C}_D$ and lift coefficient C_L for $\Omega = 2$ and $f = 2.5$. Blue line – LES, red – RSM HJ, adopted from Palkin et al. (2018). (For interpretation of the references to colour in this figure legend, the reader is referred to the web version of this article.)

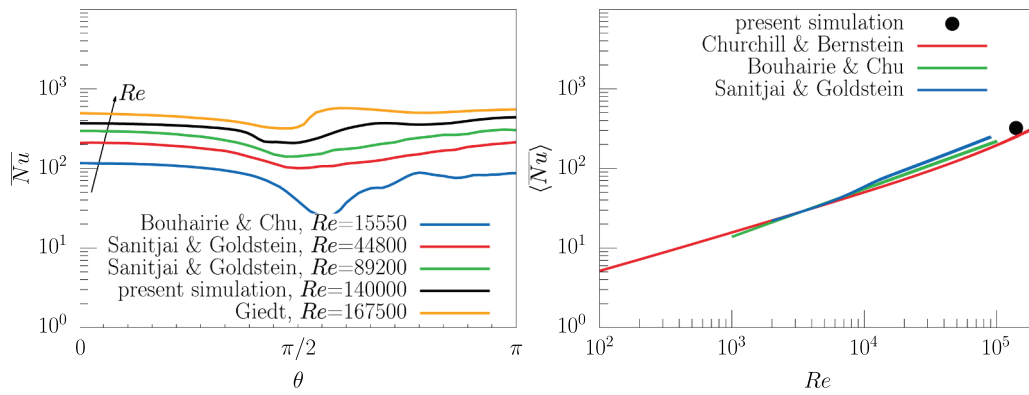


Fig. 3. Left: Circumferential profile of the time-averaged Nusselt number $\bar{Nu}(\theta)$ for non-rotating cylinder compared to experimental and numerical results (Bouhairie and Chu, 2007; Sanitjai and Goldstein, 2004; Giedt, 1951). Right: The overall Nusselt number $\langle \bar{Nu} \rangle$ as a function of the Reynolds number compared to empirical correlations from the literature, see (8) and (9). A correlation from Bouhairie and Chu (2007) is also shown: $\langle \bar{Nu} \rangle = 0.25Re^{0.6}Pr^{0.38}$ for $10^3 < Re < 10^5$.

time-averaged Nusselt number \bar{Nu} with the angle θ around the cylinder and $\langle \bar{Nu} \rangle$ compared with data from the literature, where $\langle \rangle$ stands for the averaging over the surface of the cylinder as mentioned above. At the frontal stagnation point, \bar{Nu} agrees very well with the correlation proposed by Sanitjai and Goldstein (2004) within less than 1% difference. However, the average Nusselt number is somewhat higher than predicted by the empirical correlations proposed by Churchill and Bernstein (1977) for the range $Re = 10^2 - 10^7$ and $RePr > 0.2$:

$$\langle \bar{Nu} \rangle = 0.3 + \frac{0.62Re^{1/2}Pr^{1/3}}{[1 + (0.4/Pr)^{2/3}]^{1/4}} \left[1 + \frac{10^{-5}}{2.82}Re \right]^{4/5}, \quad (8)$$

but lower than the value calculated according to correlation by Sanitjai and Goldstein (2004) for the range $Re = 2 \times 10^3 - 10^5$ and $Pr = 0.7 - 176$:

$$\langle \bar{Nu} \rangle = 0.466Re^{0.5}Pr^{0.35} + 0.528Pr^{0.42} \times \left[\left(6.5 \exp \frac{Re}{5000} \right)^{-5} + (0.031Re^{0.8})^{-5} \right]^{-1/5}. \quad (9)$$

The comparison of these two empirical correlations shows significant differences for $Re = 1.4 \times 10^5$ which give $\langle \bar{Nu} \rangle \approx 253$ and 342, respectively. Note that the heat transfer is very sensitive to a number of factors such as the aspect ratio of the channel width to diameter of the cylinder leading to a systematic bias of Nu in experimental measurements (Chang and Mills, 2004) when projected on the case of a very long cylinder. Anyhow, the distribution of \bar{Nu} over the cylinder and the averaged value $\langle \bar{Nu} \rangle = 317$ obtained with RSM HJ with the GGDH heat flux model fall within the scatter of the experimental correlations, see

Fig. 3. These results together with flow field validation in the case of rotary oscillations indicate that the present method is reliable for further analysis.

3. Flow dynamics and related drag reduction

The impact of rotary oscillations on flow dynamics and integral flow parameters such as the drag force is described in the work prior to this research. Palkin et al. (2018) performed detailed analyses of the flow modifications and drag reduction mechanism due to forced rotary oscillations. Here, we will describe the main features of the flow important for understanding of heat transfer mechanism under rotary oscillations.

The cylinder rotary oscillations induce significant modification of the flow dynamics and dominant large-scale structures. The isosurfaces of the Q -criterion, where $Q = (\Omega_{ij}\Omega_{ij} - S_{ij}S_{ij})/2$ with Ω_{ij} and S_{ij} being the symmetric and asymmetric component of the velocity gradient tensor, computed for all considered cases, shown in Fig. 4, reveal that the three-dimensional coherent finger-like structures in a wide wake in the non-rotating case, are replaced by much smaller and more regular spanwise vortices in form of nearly two-dimensional rolls. These changes, observed to become stronger with the increase in Ω and f , have a profound effect on the instantaneous and mean values of the drag coefficient. The forcing frequency controls detachment of the main vortex from the cylinder wall by an opposite-sign vorticity buffer layer generated by rotation and placed between the cylinder wall and the main vortex, see Fig. 8 in Palkin et al. (2018). It also dictates the size of vortices that grow in the near-wall region as higher frequency means a

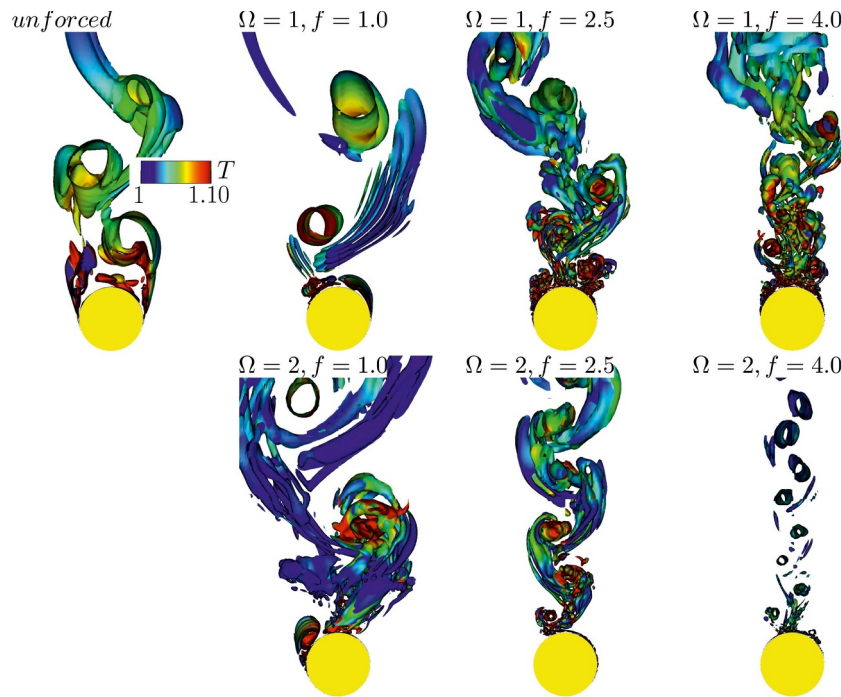


Fig. 4. Isosurface of $Q = 0.5$ for all the cases colored with the value of the instantaneous temperature field.

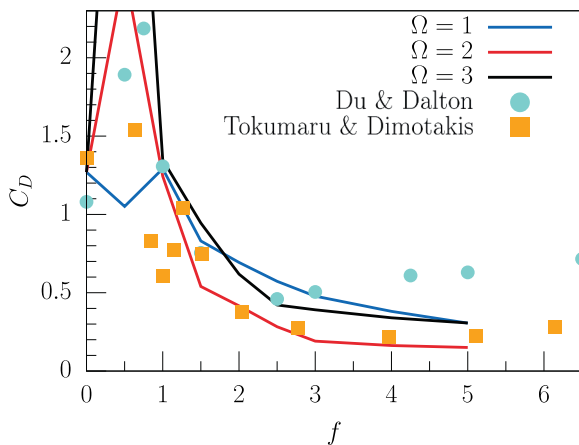


Fig. 5. C_D for different rotational frequencies and amplitudes. Lines denote our earlier results for various values of Ω and f , see Palkin et al. (2018). Numerical results by Du and Dalton (2013) are also shown as well as the experimental data by Tokumaru and Dimotakis (1991).

shorter time for their growth. The rotational amplitude, on the other hand, influences the strength and thickness of the vorticity layer that grows around the cylinder wall.

Compared to the non-rotating case, for $f = 1$ the main vortex increases in size due to combined effects of forcing frequency and rotational amplitude. As a result, the mean recirculation zone is reduced by about 40% for $\Omega = 1$ or completely vanish for $\Omega = 2$. The wake structure is well synchronized with the cylinder oscillation resulting in the increase of the drag and lift fluctuations acting on the cylinder, see Fig. 5. The picture is very different for the flow subjected to the rotational frequency of 2.5. The larger frequency reduces the time period in which the near wall vortices can grow. While for $\Omega = 1$ the flow still appears chaotic, for $\Omega = 2$ the vortex street becomes much more narrow and organized. Further increase of the forcing frequency to $f = 4$, does not produce very different flow dynamics compared to the case $f = 2.5$. Fig. 5 shows variation of the drag coefficient depending on different combinations of the rotational frequency and amplitude. The most

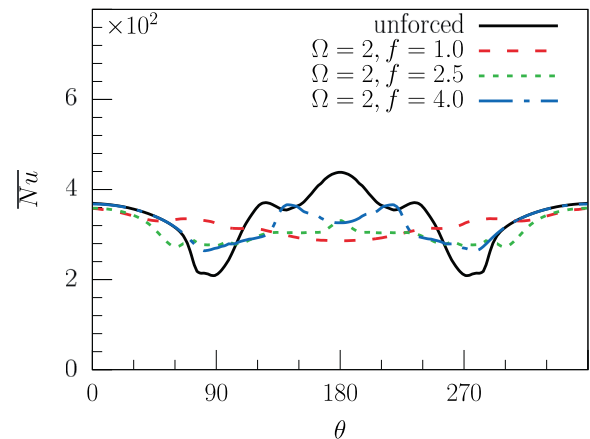
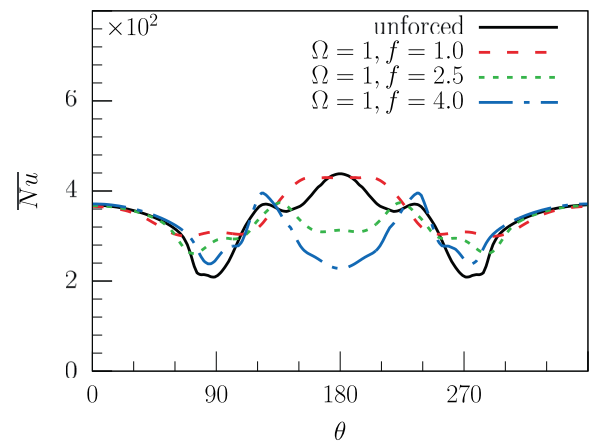


Fig. 6. Circumferential distribution of $\overline{Nu}(\theta)$ for all the cases.

dramatic drop in the drag coefficient occurs when the rotational frequency increases from 1 to 2.5 which is discussed in details by Palkin et al. (2018).

4. Temperature field and local Nusselt number

4.1. Time-averaged fields

The distribution of the time-averaged Nusselt number $\overline{Nu}(\theta)$ around the cylinder is shown in Fig. 6 demonstrating two distinguished peaks for most cases, at the front and at the rear central points of the cylinder. For the non-rotating case the rear \overline{Nu} ($\theta = 180^\circ$) is higher than the value at the front ($\theta = 0^\circ$) which characterizes the Nusselt number distribution for high Reynolds number flow (Bouhairie and Chu, 2007) mentioned in the Introduction. The way heat is transferred to the fluid in the front is very much different from the heat transfer mechanism at the back of the cylinder. The front \overline{Nu} is the result of a thin laminar boundary layer formed by impingement which grows as the fluid moves around the cylinder causing a decrease in local \overline{Nu} . The lowest value is reached roughly at the initial separation point. The heat transfer at the back region is driven by the turbulent flow characterized by large vortical structures shed alternately from the top and bottom side of the cylinder. These larger vortices grow from initially wall-attached eddies and stay in the wake region for some time before they are shed downstream.

They efficiently remove heat from the cylinder wall as recirculating fluid is thinning the thermal boundary layer and washing the heat up from the wall. The heat transfer is additionally intensified by turbulence that is transported from the turbulent shear layer, where it is produced, into the near-wake region.

The rotary oscillations of the cylinder have a notable effect on the distribution of \overline{Nu} but mainly in the separation and wake regions. The overall $\langle \overline{Nu} \rangle$ changes fall within a reasonable range depending on Ω and f , see Table 1. The mild 10% intensification is obtained for cases with $f = 1$ resembling the lock-on heat transfer increase in the laminar case (Mahfouz and Badr, 2000). For some cases the maximum value of \overline{Nu} at the back surface of the cylinder present for the non-rotating cylinder splits in two and the overall level decreases with the increase in f while for $\Omega = 2$ it is not monotonic. The circumferential distribution becomes more uniform with a flat profile at the previous location of the dip in the wake region. This feature can be used to suppress local overheats in practical applications.

4.2. Instantaneous fields

Figs. 7–10 show the instantaneous fields of spanwise vorticity ω_z and temperature T along with their circumferential profiles at two different but close time instants for unforced and forced cylinder with $\Omega = 1$ and three forcing frequencies, respectively. The results for $\Omega = 2$ are similar but also reflected in the analysis of phase-averaged fields below, thus, we consider here only $\Omega = 1$. Figs. 7a show the instant of time at which the large vortex is convected further downstream and the new main vortex is still not detached from the wall. The peak in the corresponding instantaneous local Nusselt number profile for the unforced cylinder is located close to the center of the cylinder, where the vorticity profile changes its sign at the wall. This is also pointed out by Bouhairie and Chu (2007) for an order of magnitude lower Reynolds number. At the wall the change of vorticity sign denotes the location where the tangential velocity changes its direction making a particularly thin boundary layer. The tangential fluid motion, generated by the large vortex structure, causes a strong stretching of the boundary layer leading to thinning of the thermal boundary layer and high heat

transfer rates. As the main vortex loses its strength and eventually collapses, its impact on the boundary layer becomes weaker, thus resulting in a less intensive heat transfer on the back surface and an overall smaller Nu number, see Fig. 7b. The main reason for locally high values of Nu is the interaction of the large scale vortex with the boundary layer and its interruption at the point where the tangential velocity changes its sign. This results in a particularly thin boundary layer and related high thermal gradients forcing high heat flux from the back surface. This is somewhat a different mechanism of high heat transfer rate from that described by Bouhairie and Chu (2007) where efficient removal of heat was found to occur along narrow space between two neighboring wall-attached counter rotating eddies, referred to as “flares”.

Forcing the cylinder with $\Omega = 1$ and $f = 1$ has a profound effect on the distribution of time-averaged Nu but mainly in the region where the unforced cylinder has a dip in the Nusselt number profile, see Fig. 6. While overall average Nusselt number increases around 10%, see Table 1, the main difference compared to the unforced cylinder is the disappearance of the dip in the mean Nusselt number profile. The Nu distribution is now more uniform with a flat profile at the previous location of the dip and with somewhat wider region of the maximum value at the rear. The maximum value that occurs at the back surface of the cylinder is similar to those in the unforced case. Fig. 8a shows the time instant with a wall-attached vortex on the upper half of the cylinder with a strong recirculation zone while in Fig. 8b this structure starts to detach from the wall. For the first case there is a thin thermal boundary layer at the location of the wall-attached vortex with a corresponding local peak in the Nusselt number distribution. The second peak in Nu occurs at the bottom and is a result of the flare that is formed between two counter-rotating vortices visible in the distribution of the vorticity. As the vortex detaches from the wall, Nusselt number gets lower, see Fig. 9b. The figure reveals the existence of a wall-attached opposite-sign vorticity layer generated by the rotation which traps and heats the fluid close to the wall thus reducing its heat removal capacity. As it was the case with the non-rotating cylinder, the change of the vorticity sign signals the local maximum in the Nusselt number distribution. However, other peaks in Nu shown in both Fig. 8a and b seem not to correlate with the sign change in the vorticity profile. Another interesting observation is that Nu at the front stays unaffected by rotary oscillations due to laminar regime of the boundary layer. This is a general feature of heat transfer due to conduction and locally parallel streamlines of the fluid flow, thus, the additional tangential acceleration does not significantly influence the temperature field close to the wall.

An increase of the forcing frequency to 2.5 results in a larger number of near wall eddies, shown in Fig. 9, compared to the case $f = 1$ where the corresponding flow field is dominated by the main vortex and a very few instabilities that occur in the near-wall region, see Palkin et al. (2018) for details. The time-averaged Nusselt number drops further on the back surface as shown in Fig. 6. The overall Nu decreases by 4% compared to the reference value for the unforced case. The instantaneous Nusselt number shown in Fig. 9a has two local maxima that do not occur close to 180° anymore, but they are located in the region of approximately 130° . This is also reflected in the profile of the time-averaged Nusselt number where two mild peaks exist at approximately the same location. The reduction of the heat transfer rate on the back of the cylinder is determined by the higher forcing frequency that disturbs the growth of the main vortex and results in an overall smaller size of the main coherent structure near the wall. The vorticity distribution shown in Fig. 9 is much more irregular due to large number of small scale vortices that populate the near wall region. A more pronounced peak in the instantaneous Nusselt number is due to the flare visible in the vorticity field.

A further increase in rotational frequency ($f = 4$) leads to further reduction of the vortical structures in the wake. The time-averaged Nusselt number does not change much from $\theta = 0^\circ$ till $\theta = 135^\circ$

Table 1

The value of $\langle \overline{Nu} \rangle$ for all the cases.

	$f = 1$	$f = 2.5$	$f = 4$
$\Omega = 1$	343	316	307
$\Omega = 2$	321	305	319

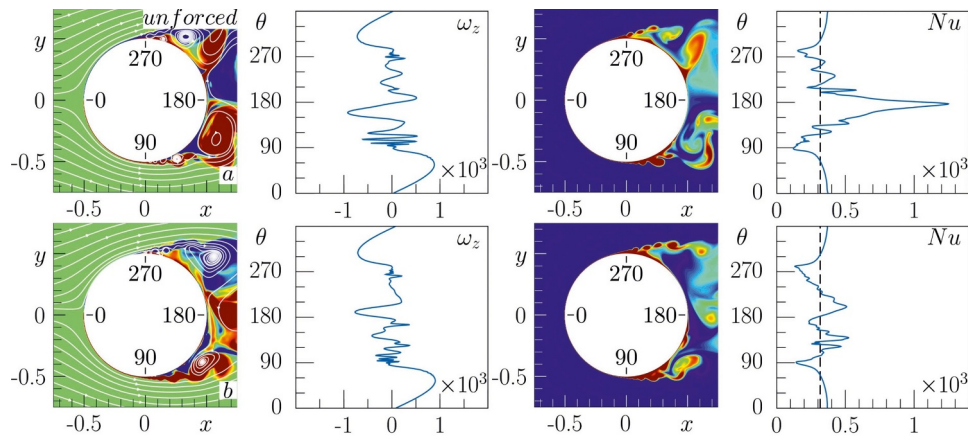


Fig. 7. Instantaneous spanwise vorticity and temperature fields with streamlines, circumferential profiles of the corresponding vorticity and Nusselt number distribution on the wall for the unforced case and two typical time instants (Top: a, bottom: b).

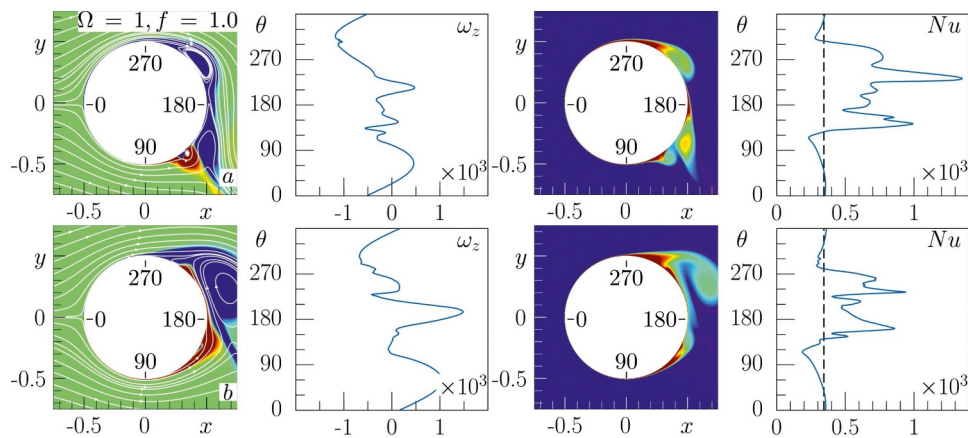


Fig. 8. Instantaneous spanwise vorticity and temperature fields with streamlines, circumferential profiles of the corresponding vorticity and Nusselt number distribution on the wall for $\Omega = 1, f = 1$ and two typical time instants (Top: a, bottom: b).

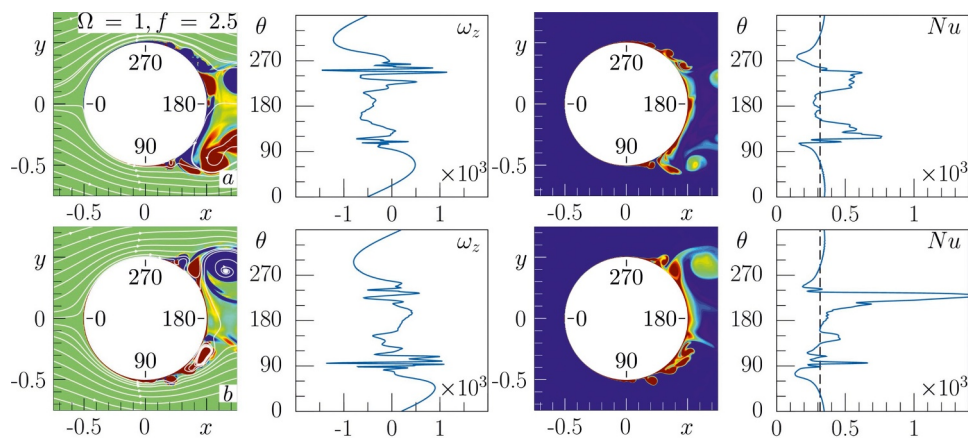


Fig. 9. Instantaneous spanwise vorticity and temperature fields with streamlines, circumferential profiles of the corresponding vorticity and Nusselt number distribution on the wall for $\Omega = 1, f = 2.5$ and two typical time instants (Top: a, bottom: b).

compared to the previous case, while \overline{Nu} number further decreases from $\theta = 135^\circ$ till 180° . The Nu distribution resembles the low Reynolds number results where the rare surface has a smaller value of Nu than the front one. This is expected as the high forcing frequency leads to a significant suppression of turbulence as reported in Palkin et al. (2018). Instantaneous fields shown in Fig. 10 show more uniform distribution of Nu at the back surface and absence of large scale coherent structures strong enough to cause modification of the boundary layer as observed in the previous cases.

4.3. Phase-averaged fields

Fig. 11 shows the two-dimensional distribution of the phase-averaged temperature field for the non-rotating case (first row) and for $\Omega = 1$ with three considered frequencies (three bottom rows) at two different phases. In the case of unforced cylinder two phases correspond to the maximum (left) and zero (right) value of the lift coefficient C_L . The temperature field is transported in a wide turbulent wake reflected in large oscillations of the instantaneous and phase-averaged Nusselt number and spanwise vorticity

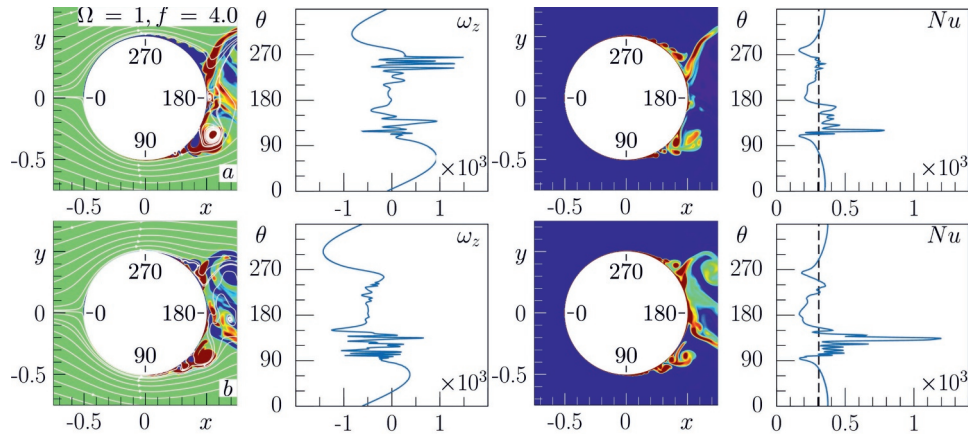


Fig. 10. Instantaneous spanwise vorticity and temperature fields with streamlines, circumferential profiles of the corresponding vorticity and Nusselt number distribution on the wall for $\Omega = 1$, $f = 4$ and two typical time instants (Top: a, bottom: b).

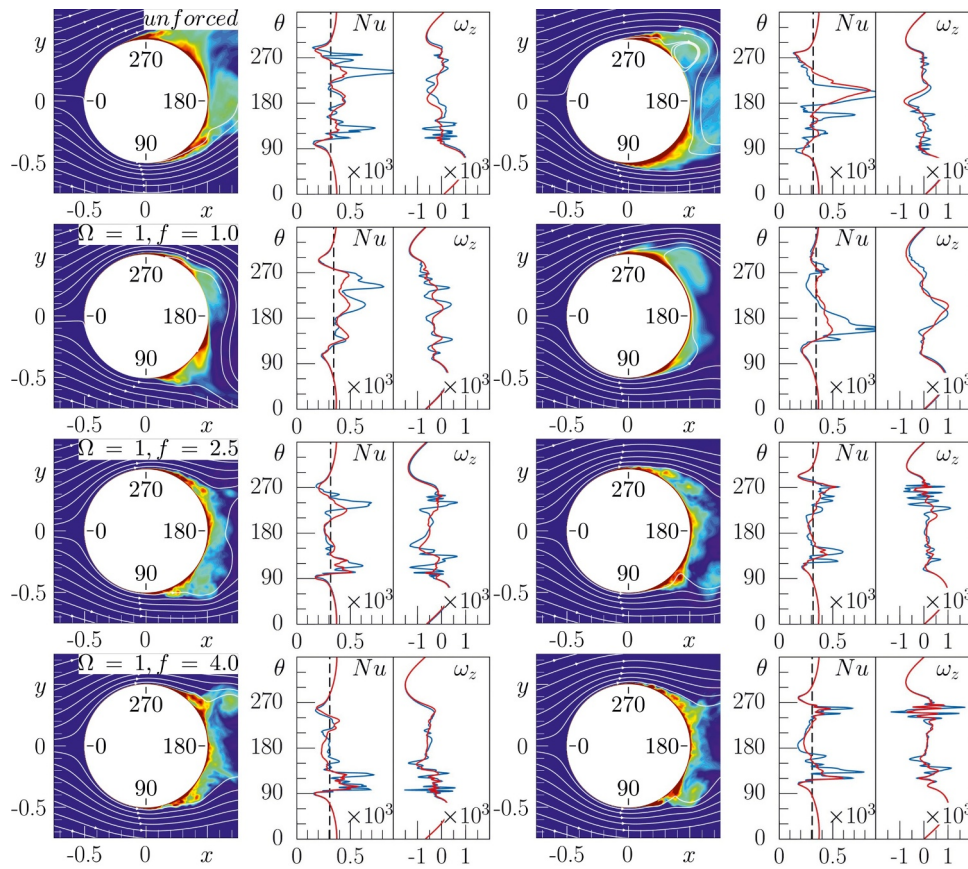


Fig. 11. Phase-averaged temperature field with streamlines, circumferential profiles of the phase-averaged (red line) and corresponding instantaneous (blue line) profiles of the Nusselt number and spanwise vorticity for $\Omega = 1$. Left: phase $\varphi = \pi/2$, right: $\varphi = \pi$. (For interpretation of the references to colour in this figure legend, the reader is referred to the web version of this article.)

ω_z at the wall. These plots again demonstrate how the separation appearing at about $\theta \approx 90^\circ$ and 270° weakens the local heat transfer, while the energetic vortical structure intensifies it due to a thinning local thermal boundary layer (rear point, $\theta = 180^\circ$).

In the case of rotary oscillations we consider two phases according to Eq. (1), i.e. $\varphi = \pi/2$ and π , which generally describe the whole oscillation period since $\varphi = 3\pi/2$ and 2π are $y \rightarrow -y$ symmetric with respect to $\varphi \rightarrow \varphi + \pi$. The case $f = 1$ features a similar high amplitude deviations of Nu and ω_z compared to the unforced case. With a significant increase in f the wake and the heated area behind the cylinder become more localized compared to the unforced case, see also Fig. 4.

The profiles of the Nusselt number and vorticity show less deviations from period to period. This periodicity allows to recognize a phase-averaged near-wall vortical train appearing as wiggles on the profiles of Nu and ω_z , see $\varphi = \pi$ for $\Omega = 1$, $f = 4$. These observations become even more pronounced for $\Omega = 2$ where the instantaneous and phase-averaged profiles are very close, see Fig. 12.

5. Conclusion

We performed heat transfer computations of a flow over a rotary oscillating infinite heated cylinder for a high subcritical Reynolds

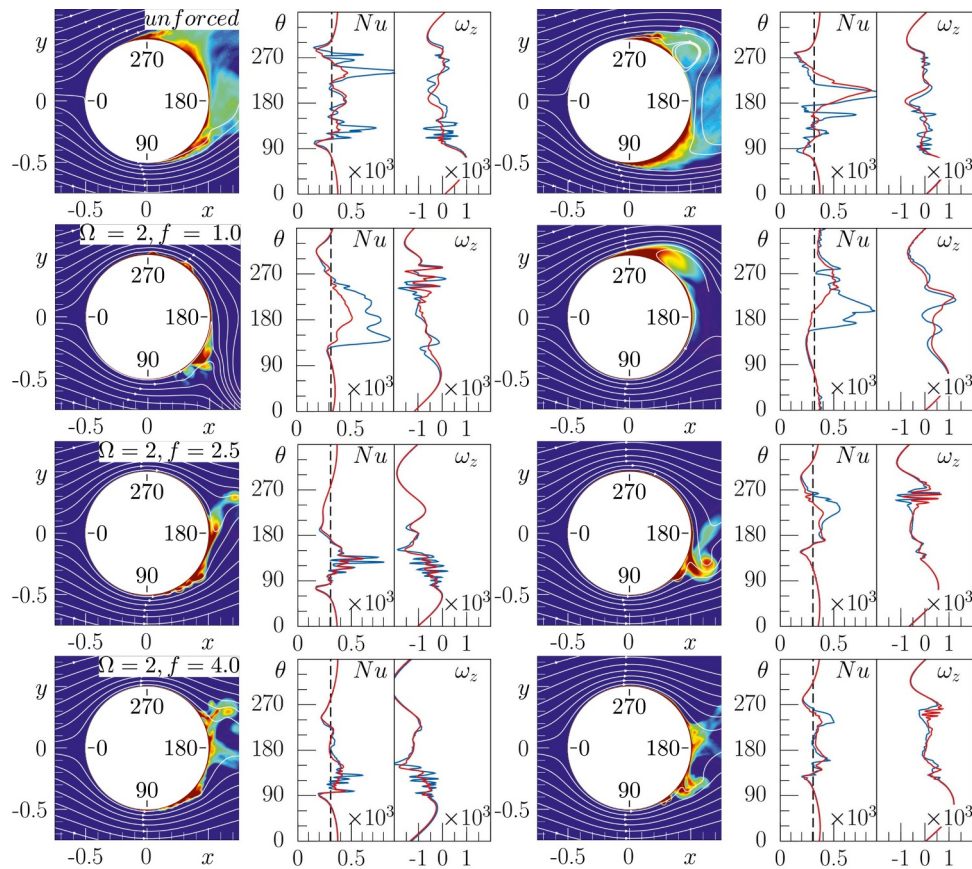


Fig. 12. Phase-averaged temperature field with streamlines, circumferential profiles of the phase-averaged (red line) and corresponding instantaneous (blue line) profiles of the Nusselt number and spanwise vorticity for $\Omega = 2$. Left: phase $\varphi = \pi/2$, right: $\varphi = \pi$. (For interpretation of the references to colour in this figure legend, the reader is referred to the web version of this article.)

number $Re = 1.4 \times 10^5$, two forcing amplitudes $\Omega = 1, 2$ and three frequencies $f = 1, 2.5$ and 4 . The parametric study was performed by solving three-dimensional unsteady Reynolds-averaged Navier–Stokes (URANS) momentum and energy equations, closed respectively by a validated wall-integrated second-moment (Re-stress) and an anisotropic (GGDH) eddy-diffusivity model. The general observation is that the overall heat transfer at relatively high frequencies does not significantly differ from the non-rotating (unforced) case. At the same time for $f = 1$ the overall Nusselt number increases by some 10% which is in line with the previous observations for laminar low Re regimes close to the lock-on boundary (Mahfouz and Badr, 2000). However, this study focused mainly on rapidly oscillating cases which were previously found efficient for the drag reduction (Palkin et al., 2018). As the method of rotary oscillations was first found appealing for drag reduction and suppression of energetic periodic oscillations, it also appears efficient in reducing peaks in heat transfer that appear locally from the cylinder surface. A notable consequence of the rotary oscillating forcing is a more uniform angular distribution of Nu as shown in Fig. 6. This could be potentially an interesting finding as many practical applications try to avoid local overheat and hot spots that could lead to thermal fatigue and the consequent structural damages of materials and devices.

The main conclusions are summarized as follows:

- For the unforced cylinder, heat transfer is characterized by the occurrence of very high local heat transfer rate due to efficient thinning of the thermal boundary layer as a result of interaction of large coherent structures that appear periodically in the near-wake region.
- The high peaks in the Nu number profile occur at the locations

where the tangential velocity changes its sign resulting in a thin boundary layer.

- The dip in the Nusselt number is caused by the local periodic separation on the wall and the resulting thickening of the thermal boundary layer. The recirculating fluid becomes trapped and heated, thus, reducing the heat transfer rates.
- Forcing the cylinder rotation with $\Omega = 1, 2$ and $f = 1$ results in a somewhat larger overall Nusselt number as the main vortex, enhanced by rotation, gets larger and stronger.
- Higher frequencies, 2.5 and 4 , lead to a diminishing in the overall Nusselt number due to reduction in the size and strength of the main coherent structures. The circumferential distribution of Nu becomes more uniform with less frequent occurrence of high values.

Acknowledgment

The work is supported by Russian Foundation for Basic Research grant No. 18-38-20167. The development of the heat transfer model is performed under the state contract with IT SB RAS. The computational resources are provided by Novosibirsk State University Computing Centre (Novosibirsk), Siberian Supercomputer Centre SB RAS (Novosibirsk) and Joint Supercomputer Centre RAS (Moscow).

Supplementary material

Supplementary material associated with this article can be found, in the online version, at [10.1016/j.ijheatfluidflow.2019.108441](https://doi.org/10.1016/j.ijheatfluidflow.2019.108441).

References

- Aguedal, L., Semmar, D., Berrouk, A., Azzi, A., Oualli, H., 2018. 3d vortex structure investigation using large eddy simulation of flow around a rotary oscillating circular cylinder. *Eur. J. Mech./B Fluids* 71, 113–125.
- Al-Mdallal, Q., Mahfouz, F., 2017. Heat transfer from a heated non-rotating cylinder performing circular motion in a uniform stream. *Int. J. Heat Mass Transfer* 112, 147–157.
- Armaly, B., Madsen, D., 1971. Heat transfer from an oscillating horizontal wire. *J. Heat Transfer* 93 (2), 239–240.
- Baughn, J., Saniei, N., 1991. The effect of the thermal boundary condition on heat transfer from a cylinder in crossflow. *J. Heat Transfer* 113 (4), 1020–1022.
- Beskok, A., Raisee, M., Celik, B., Yagiz, B., Cheraghi, M., 2012. Heat transfer enhancement in a straight channel via a rotationally oscillating adiabatic cylinder. *Int. J. Therm. Sci.* 58, 61–69.
- Bloor, M., 1964. The transition to turbulence in the wake of a circular cylinder. *J. Fluid Mech.* 19 (2), 290–304.
- Bouhairie, S., Chu, V., 2007. Two-dimensional simulation of unsteady heat transfer from a circular cylinder in crossflow. *J. Fluid Mech.* 570, 177–215.
- Boulos, M., Pei, D., 1974. Dynamics of heat transfer from cylinders in a turbulent air stream. *Int. J. Heat Mass Transfer* 17 (7), 767–783.
- Cantwell, B., Coles, D., 1983. An experimental study of entrainment and transport in the turbulent near wake of a circular cylinder. *J. Fluid Mech.* 136, 321–374.
- Celik, B., Akdag, U., Gunes, S., Beskok, A., 2008. Flow past an oscillating circular cylinder in a channel with an upstream splitter plate. *Phys. Fluids* 20 (10), 103603.
- Celik, B., Beskok, A., 2009. Mixing induced by a transversely oscillating circular cylinder in a straight channel. *Phys. Fluids* 21 (7), 073601.
- Chang, B., Mills, A., 2004. Effect of aspect ratio on forced convection heat transfer from cylinders. *Int. J. Heat Mass Transfer* 47 (6–7), 1289–1296.
- Cheng, C., Chen, H., Aung, W., 1997. Experimental study of the effect of transverse oscillation on convection heat transfer from a circular cylinder. *J. Heat Transfer* 119 (3), 474–482.
- Cheng, W., Pullin, D., Samtaney, R., Zhang, W., Gao, W., 2017. Large-eddy simulation of flow over a cylinder with Re_d from 3.9×10^3 to 8.5×10^5 : a skin-friction perspective. *J. Fluid Mech.* 820, 121–158.
- Choi, H., Jeon, W., Kim, J., 2008. Control of flow over a bluff body. *Annu. Rev. Fluid Mech.* 40, 113–139.
- Churchill, S., Bernstein, M., 1977. A correlating equation for forced convection from gases and liquids to a circular cylinder in crossflow. *J. Heat Transfer* 99 (2), 300–306.
- Deaver, F., Penney, W., Jefferson, T., 1962. Heat transfer from an oscillating horizontal wire to water. *J. Heat Transfer* 84 (3), 251–254.
- Du, L., Dalton, C., 2013. Les calculation for uniform flow past a rotationally oscillating cylinder. *J. Fluids Struct.* 42, 40–54.
- Durbin, P., 1996. On the $k-\epsilon$ stagnation point anomaly. *Int. J. Heat Fluid Flow* 17, 9–90.
- Fage, A., 1929. The effects of turbulence and surface roughness on the drag of a circular cylinder. *Rep. Memo.* 1.
- Faircloth, J., Schaetzle, W., 1969. Effect of vibration on heat transfer for flow normal to a cylinder. *J. Heat Transfer* 91 (1), 140–144.
- Fu, W., Tong, B., 2002. Numerical investigation of heat transfer from a heated oscillating cylinder in a cross flow. *Int. J. Heat Mass Transfer* 45 (14), 3033–3043.
- Gau, C., Wu, J., Liang, C., 1999. Heat transfer enhancement and vortex flow structure over a heated cylinder oscillating in the crossflow direction. *J. Heat Transfer* 121 (4), 789–795.
- Giedt, W., 1951. Effect of turbulence level of incident air stream on local heat transfer and skin friction on a cylinder. *J. Aeronaut. Sci.* 18 (11), 725–730.
- Hadžiabdić, M., Hanjalić, K., 2008. Vortical structures and heat transfer in a round impinging jet. *J. Fluid Mech.* 596, 221–260.
- Hilpert, R., 1933. Wärmeabgabe von geheizten drähten und rohren im luftstrom. *Forsch. Gebiete. Ingenieurw.* 4 (5), 215–224.
- Ince, N.Z., Launder, B.E., 1989. On the computation of buoyancy-driven turbulent flows in rectangular enclosures. *Int. J. Heat Fluid Flow* 10 (2), 110–117.
- Jakirlić, S., Hanjalić, K., 2002. A new approach to modelling near-wall turbulence energy and stress dissipation. *J. Fluid Mech.* 459, 139–166.
- Jameson, G., 1964. Mass (or heat) transfer from an oscillating cylinder. *Chem. Eng. Sci.* 19 (10), 793–800.
- Karanth, D., Rankin, G., Sridhar, K., 1994. A finite difference calculation of forced convective heat transfer from an oscillating cylinder. *Int. J. Heat Mass Transfer* 37 (11), 1619–1630.
- Karniadakis, G., Triantafyllou, G., 1992. Three-dimensional dynamics and transition to turbulence in the wake of bluff objects. *J. Fluid Mech.* 238, 1–30.
- Kruzhilin, G., 1936. A theory of heat transfer for a circular cylinder in cross flow. *J. Tekhn. Fiz.* 6 (5), 858–865.
- Lehmkuhl, O., Rodríguez, I., Borrell, R., Chiva, J., Oliva, A., 2014. Unsteady forces on a circular cylinder at critical reynolds numbers. *Phys. Fluids* 26 (12), 125110.
- Lemlich, R., 1955. Effect of vibration on natural convective heat transfer. *Ind. Eng. Chem.* 47 (6), 1175–1180.
- Lemlich, R., Levy, M., 1961. The effect of vibration on natural convective mass transfer. *AIChE J.* 7 (2), 240–242.
- Lemlich, R., Rao, M., 1965. The effect of transverse vibration on free convection from a horizontal cylinder. *Int. J. Heat Mass Transfer* 8 (1), 27–33.
- Leung, C., Ko, N., Ma, K., 1981. Heat transfer from a vibrating cylinder. *J. Sound Vib.* 75 (4), 581–582.
- Mahfouz, F., Badr, H., 1999. Heat convection from a cylinder performing steady rotation or rotary oscillation—part i: rotary oscillation. *Heat Mass Transfer* 34 (5), 375–380.
- Mahfouz, F., Badr, H., 2000. Forced convection from a rotationally oscillating cylinder placed in a uniform stream. *Int. J. Heat Mass Transfer* 43 (17), 3093–3104.
- Manceau, R., Perrin, R., Hadžiabdić, M., Benhamadouche, S., 2014. Investigation of the interaction of a turbulent impinging jet and a heated, rotating disk. *Phys. Fluids* 26 (3), 035102.
- Medic, G., Durbin, P., 2002. Toward improved prediction of heat transfer on turbine blades. *J. Turbomach.* 124 (2), 187–192.
- Mittal, H., Al-Mdallal, Q., 2018. A numerical study of forced convection from an isothermal cylinder performing rotational oscillations in a uniform stream. *Int. J. Heat Mass Transfer* 127, 357–374.
- Morgan, V., 1975. The overall convective heat transfer from smooth circular cylinders. *Advances in Heat Transfer*. 11. Elsevier, pp. 199–264.
- Ničeno, B., Hanjalić, K., 2005. Unstructured large eddy and conjugate heat transfer simulations of wall-bounded flows. *Model. Simul. Turbul. Heat Transfer* 32–73.
- Ničeno, B., Palkin, E., Mullyadzhano, R., Hadžiabdić, M., Hanjalić, K., 2018. T-Flows Web page. <https://github.com/DeNov/T-Flows>.
- Nobari, M., Ghazanfarian, J., 2010. Convective heat transfer from a rotating cylinder with inline oscillation. *Int. J. Therm. Sci.* 49 (10), 2026–2036.
- Palkin, E., Hadžiabdić, M., Mullyadzhano, R., Hanjalić, K., 2018. Control of flow around a cylinder by rotary oscillations at a high subcritical reynolds number. *J. Fluid Mech.* 855, 236–266.
- Palkin, E., Mullyadzhano, R., Hadžiabdić, M., Hanjalić, K., 2016. Scrutinizing urans in shedding flows: the case of cylinder in cross-flow in the subcritical regime. *Flow Turbul. Combust.* 97 (4), 1017–1046.
- Papell, S., 1981. Influence of thermal boundary conditions on heat transfer from a cylinder in cross flow.
- Park, H., Gharib, M., 2001. Experimental study of heat convection from stationary and oscillating circular cylinder in cross flow. *J. Heat Transfer* 123 (1), 51–62.
- Perkins Jr, H., Leppert, G., 1964. Local heat-transfer coefficients on a uniformly heated cylinder. *Int. J. Heat Mass Transfer* 7 (2), 143–158.
- Pottebaum, T., Gharib, M., 2006. Using oscillations to enhance heat transfer for a circular cylinder. *Int. J. Heat Mass Transfer* 49 (17–18), 3190–3210.
- Rodríguez, I., Lehmkuhl, O., Chiva, J., Borrell, R., Oliva, A., 2015. On the flow past a circular cylinder from critical to super-critical reynolds numbers: wake topology and vortex shedding. *Int. J. Heat Fluid Flow* 55, 91–103.
- Roshko, A., 1954. On the drag and shedding frequency of two-dimensional bluff bodies. *Report No.*, 1191. NACA.
- Roshko, A., 1961. Experiments on the flow past a circular cylinder at very high reynolds number. *J. Fluid Mech.* 10 (3), 345–356.
- Sak, C., Liu, R., Ting, D., Rankin, G., 2007. The role of turbulence length scale and turbulence intensity on forced convection from a heated horizontal circular cylinder. *Exp. Therm. Fluid. Sci.* 31 (4), 279–289.
- Sanitjai, S., Goldstein, R., 2004. Forced convection heat transfer from a circular cylinder in crossflow to air and liquids. *Int. J. Heat Mass Transfer* 47 (22), 4795–4805.
- Saxena, U., Laird, A., 1978. Heat transfer from a cylinder oscillating in a cross-flow. *J. Heat Transfer* 100 (4), 684–689.
- Schmidt, E., Wenner, K., 1941. Heat transfer over the circumference of a heated cylinder in transverse flow (12), 65–73.
- Sellappan, P., Pottebaum, T., 2014. Vortex shedding and heat transfer in rotationally oscillating cylinders. *J. Fluid Mech.* 748, 549–579.
- Shiels, D., Leonard, A., 2001. Investigation of a drag reduction on a circular cylinder in rotary oscillation. *J. Fluid Mech.* 431, 297–322.
- Singh, S., Mittal, S., 2005. Flow past a cylinder: shear layer instability and drag crisis. *Int. J. Numer. Methods Fluids* 47 (1), 75–98.
- Small, J., 1935. Xx. the average and local rates of heat transfer from the surface of a hot cylinder in a transverse stream of fluid. *Phil. Mag.* 19 (125), 251–260.
- Sparrow, E., Abraham, J., Tong, J., 2004. Archival correlations for average heat transfer coefficients for non-circular and circular cylinders and for spheres in cross-flow. *Int. J. Heat Mass Transfer* 47 (24), 5285–5296.
- Sreenivasan, K., Ramachandran, A., 1961. Effect of vibration on heat transfer from a horizontal cylinder to a normal air stream. *Int. J. Heat Mass Transfer* 3 (1), 60–67.
- Thielen, L., Hanjalić, K., Jonker, H., Manceau, R., 2005. Predictions of flow and heat transfer in multiple impinging jets with an elliptic-blending second-moment closure. *Int. J. Heat Mass Transfer* 48 (8), 1583–1598.
- Thom, A., 1933. The flow past circular cylinders at low speeds. *Proc. R. Soc.* 141 (845), 651–669.
- Tokumar, P., Dimotakis, P., 1991. Rotary oscillation control of a cylinder wake. *J. Fluid Mech.* 224, 77–90.
- Wieselsberger, C., 1922. New data on the laws of fluid resistance.
- Williamson, C., 1988. The existence of two stages in the transition to three-dimensionality of a cylinder wake. *Phys. Fluids* 31 (11), 3165–3168.
- Xia, M., Karniadakis, G., 1997. Three-dimensional modeling of unsteady heat transfer. *ASME Fluids Engineering Division Summer Meeting*. pp. 1–6.
- Zijnen, B., 1958. Heat transfer from horizontal cylinders to a turbulent air flow. *Appl. Sci. Res. Sect. A* 7 (2–3), 205–223.
- Žukauskas, A., 1972. Heat transfer from tubes in crossflow. *Advances in Heat Transfer*. 8. Elsevier, pp. 93–160.